RESEARCH ARTICLE

Key Points:
- Aragonite saturation is primarily driven by photosynthesis and respiration-remineralization in the water column of the Gulf of Maine
- Calcium carbonate dissolution appears to occur from fall to winter in the deep portion of the Gulf of Maine
- Consistent undersaturation of subsurface aragonite saturation is likely to occur in 30–40 years under acidification in the Gulf of Maine

Correspondence to:
Z. A. Wang,
zawang@whoi.edu

Seasonal controls of aragonite saturation states in the Gulf of Maine

Zhaohui Aleck Wang [ID][1], **Gareth L. Lawson**[2], **Cynthia H. Pilskaln** [ID][3], and **Amy E. Maas** [ID][4]

[1]Department of Marine Chemistry and Geochemistry, Woods Hole Oceanographic Institution, Woods Hole, Massachusetts, USA, [2]Biology Department, Woods Hole Oceanographic Institution, Woods Hole, Massachusetts, USA, [3]School for Marine Science and Technology, University of Massachusetts Dartmouth, New Bedford, Massachusetts, USA, [4]Bermuda Institute of Ocean Sciences, St. George's, Bermuda

Abstract The Gulf of Maine (GoME) is a shelf region especially vulnerable to ocean acidification (OA) due to natural conditions of low pH and aragonite saturation states (Ω-Ar). This study is the first to assess the major oceanic processes controlling seasonal variability of the carbonate system and its linkages with pteropod abundance in Wilkinson Basin in the GoME. Two years of seasonal sampling cruises suggest that water-column carbonate chemistry in the region undergoes a seasonal cycle, wherein the annual cycle of stratification-overturn, primary production, respiration-remineralization and mixing all play important roles, at distinct spatiotemporal scales. Surface production was tightly coupled with remineralization in the benthic nepheloid layer during high production seasons, which results in occasional aragonite undersaturation. From spring to summer, carbonate chemistry in the surface across Wilkinson Basin reflects a transition from a production-respiration balanced system to a net autotropic system. Mean water-column Ω-Ar and abundance of large thecosomatous pteropods show some correlation, although patchiness and discrete cohort reproductive success likely also influence their abundance. Overall, photosynthesis-respiration is the primary driving force controlling Ω-Ar variability during the spring-to-summer transition as well as over the seasonal cycle. However, calcium carbonate ($CaCO_3$) dissolution appears to occur near bottom in fall and winter when bottom water Ω-Ar is generally low but slightly above 1. This is accompanied by a decrease in pteropod abundance that is consistent with previous $CaCO_3$ flux trap measurements. The region might experience persistent subsurface aragonite undersaturation in 30–40 years under continued ocean acidification.

1. Introduction

Ocean acidification (OA) due to rising atmospheric CO_2 [*Caldeira*, 2007; *Doney et al.*, 2009; *Orr et al.*, 2005] is considered to be more complex to measure and study in coastal regions than in the open ocean because many other processes, such as eutrophication-induced deoxygenation, inputs of low pH river water, and upwelling, may contribute significantly to lowering pH and calcium carbonate ($CaCO_3$) saturation state [*Alin et al.*, 2012; *Cai et al.*, 2011; *Feely et al.*, 2010; *Salisbury et al.*, 2008a]. The multifactored nature of coastal ocean acidification makes it difficult to understand and predict, yet it directly affects human activities and coastal resources, making it a threat to coastal ocean sustainability [*Barton et al.*, 2015; *Breitburg et al.*, 2015; *Cooley and Doney*, 2009; *Cooley et al.*, 2011; *Sutton et al.*, 2016; *Turley et al.*, 2010].

Certain coastal systems are naturally more susceptible to the effects of OA, such as the upwelling system along the U.S. West Coast, where water pH and $CaCO_3$ saturation are already low [*Alin et al.*, 2012; *Feely et al.*, 2008; *McLaughlin et al.*, 2015]. Recent studies indicate that the U.S. Northeast region is another place that is more prone to acidification [*Wang et al.*, 2013; *Wanninkhof et al.*, 2015]. Coastal waters in this region have, on average, lower pH and aragonite saturation state (Ω-Ar) as well as lower buffering capacity (as indicated by a low ratio of total alkalinity to dissolved inorganic carbon) but higher CO_2 fugacity ($f CO_2$) than more southern U.S. coastal regions. The Gulf of Maine (GoME) may be of particular concern in this regard as its shelf water displays the lowest mean in-situ pH, Ω-Ar, and buffering capacity along the East Coast in summer. Such conditions are consistent with the GoME's relatively low temperature and thus high CO_2 solubility [*Wang et al.*, 2013], inputs of fresher and low alkalinity water traceable to the rivers discharging into the Labrador Sea in the north [*Cai et al.*, 2010; *Wang et al.*, 2013], local inputs of low pH river water [*Salisbury et al.*,

2008a], and semienclosed nature (water mass residence time $\sim$1 year above 100 m; $\sim$1.5 years below 100 m) [*Brown and Beardsley*, 1978] which provides the opportunity for the accumulation of respiratory products, i.e., CO_2.

The CO_2 system in the GoME has received increased attention in the past decade [*Hales et al.*, 2008; *Najjar et al.*, 2012]. Riverine inputs of dissolved inorganic carbon (DIC) in the GoME are relatively small [*Cai et al.*, 2010; *Najjar et al.*, 2012]. The coastal areas influenced by river plumes are productive, which often causes a CO_2 sink at the surface in spring and summer [*Salisbury et al.*, 2009, 2008b]. The western GoME near Wilkinson Basin experiences a large biological uptake of CO_2 associated with regular spring blooms, but this seasonal gain is offset by fall-to-winter vertical mixing and CO_2 efflux [*Vandemark et al.*, 2011]. The annual mean efflux was estimated to be 0.01 – 0.38 mol m^{-2} yr^{-1} over multiple years with moderate interannual variability [*Signorini et al.*, 2013; *Vandemark et al.*, 2011]. Anthropogenic forces, notably atmospheric CO_2 increase and freshening due to increased inputs from sub-Arctic regions [*Townsend et al.*, 2015] are potentially combined to push seawater pH and $CaCO_3$ saturation lower in the GoME, although direct evidence of these effects has yet to be seen.

To date, OA studies have focused heavily on biological effects, especially calcification in shell-forming organisms, while the effects of OA on the inorganic carbon cycle via $CaCO_3$ dissolution have been relatively less studied [*Andersson et al.*, 2014; *Eyre et al.*, 2014]. The latter is mostly a chemical process and is expected to increase globally, although how much of an increase will occur is uncertain and the feedbacks involved are complex [*Berelson et al.*, 2007; *Broecker*, 2009; *Eyre et al.*, 2014; *Millero*, 2007; *Morse et al.*, 2007]. Understanding of variation of $CaCO_3$ saturation and its impacts on the $CaCO_3$ cycle (e.g., dissolution and calcification) in the water column of the productive Gulf of Maine is lacking, although the GoME has been identified as a "vulnerable" region for OA effects and supports rich water-column and benthic $CaCO_3$-bearing communities [*Gledhill et al.*, 2015; *Wang et al.*, 2013]. Evidence is emerging, however, suggesting dissociation of aragonite might occur. In the deep basins of the GoME, although during fall and winter thecosomatous pteropods are collected in abundance in traps deployed at depths of $\sim$100–150 m, pteropod aragonite shells are not observed in traps at depths 20–30 m above the bottom and within the benthic nepheloid layer (BNL) [*Hayashi*, 2014; *Pilskaln et al.*, 2014a]. This, coupled with a significant depth-related decrease of up to 20% between 100–150 m and 200–250 m in the $CaCO_3$ content of synchronously collected biweekly trap samples in the GoME basins [*Hayashi*, 2014], suggests aragonite dissolution at depth in fall and winter. In addition, long-term changes of biogeochemical properties, including a decrease in surface water biogenic carbonate production has also been documented in the GoME [*Balch et al.*, 2012].

The aragonite shell-forming thecosomatous pteropods (henceforth referred to as pteropods) are particularly vulnerable to acidification and represent a dominant water-column repository of aragonite. Both laboratory and field studies examining the effect of OA on live pteropods have demonstrated detrimental effects on shells under enhanced CO_2 [*Bednarsek et al.*, 2014, 2012; *Comeau et al.*, 2010]. Pteropods can be significant consumers of primary production, and also serve as key food for fish, seabirds and whales [*Armstrong et al.*, 2005; *Bernard and Froneman*, 2009; *Hunt et al.*, 2008; *Karnovsky et al.*, 2008; *Lalli and Gilmer*, 1989]. Dissolution of pteropod aragonite shells may contribute substantially to the $CaCO_3$ budget in the deep ocean and sediments and significantly affects the ocean's alkalinity budget [*Berelson et al.*, 2007; *Broecker*, 2009; *Feely et al.*, 2004]. In the GoME, *Limacina retroversa* is by far the most common pteropod species and may be among the first pelagic organisms to experience the consequences of aragonite undersaturation. Like other pteropods, *L. retroversa* has an organic periostracum covering a thin aragonite shell, and laboratory exposure experiments have shown that its shell is sensitive to undersaturation [*Lischka and Riebesell*, 2012]. Additionally, *L. retoversa* likely plays an important role in carbon biogeochemistry in the GoME via its shell calcification and dissolution. These attributes make *L. retroversa* an interesting species to study interactions with and sensitivity to changes in the carbonate chemistry of the GoME ecosystem.

This study is the first to examine seasonal variability of carbonate chemistry and aragonite saturation state in the full water column of a deep coastal region in the western Gulf of Maine off the US Northeast Coast. The 2 years of seasonal data collected in this study include concurrent in situ sampling of hydrographic and carbonate chemistry parameters and pteropod abundance. The goal is to examine individual mechanistic drivers, including physical and biogeochemical factors and processes, of carbonate parameters, particularly aragonite saturation state over the 2 year period in Wilkinson Basin and nearby banks. An in-depth analysis is conducted to investigate the spring-summer transition period, when biological productivity and subsequent remineralization are at the annual maximum. Potential $CaCO_3$ dissolution in the water column is

studied by assessing the relative contribution of different processes to variability in CO_2 parameters. We also examine linkages between carbonate chemistry and pteropod distribution. The results are used prospectively to consider changes in aragonite saturation state and potential ecological effects under ocean acidification in coming decades.

2. Methods

2.1. Study Site

The Gulf of Maine is a semienclosed continental shelf sea, isolated from the open ocean waters of the Northwest Atlantic by Georges and Browns Bank and with exchange at depth limited to the Northeast Channel [*Townsend et al.*, 2014]. Three large and deep basins (Georges, Jordan, and Wilkinson Basins) reach depths in excess of 300 m and are separated by shallower banks that link the Northeast Channel to the Gulf's interior. Local river inputs have pronounced nearshore effects [*Hunt et al.*, 2011; *Salisbury et al.*, 2009]. The Merrimack River is adjacent to the north of the study region and a few small rivers discharge into Massachusetts Bay. The study area is located in the southwestern portion of Wilkinson Basin in the western GoME (Figure 1). Mean circulation in the GoME is cyclonic, associated with a coastal limb of the Labrador Current [*Pettigrew et al.*, 2005; *Townsend et al.*, 2010]. The Western Maine Coastal Current flows southeastward through the study area and delivers material and freshwater from the north. Wilkinson Basin is generally representative of the open western gulf, exhibiting a primarily cyclonic circulation pattern. It is isolated from major direct river input. The region is characterized by strong tides and tidally-driven vertical mixing.

The GoME system experiences a distinct seasonal pattern of phytoplankton production driven by stratification dynamics and mixing [*Bigelow*, 1924; *Thomas et al.*, 2003]. Large phytoplankton blooms typically occur in the spring as increasing day length provides light; warming enhances stratification which strengthens throughout the summer. Surface cooling and enhanced wind mixing in the fall leads to the breakdown in stratification, deep water column overturn, and transport of nutrients to the surface and promotion of a fall phytoplankton bloom. In winter, the water column is generally well mixed. Particulate matter export peaks in the late spring and fall following the major plankton blooms [*Keigwin and Pilskaln*, 2015; *McGillicuddy et al.*, 2014; *Pilskaln et al.*, 2014b]. Additionally, pervasive and prominent BNLs are found throughout the GoME, maintained by tidal mixing, bottom resuspension and seasonal delivery of plankton-derived particulates from the overlying water column [*Pilskaln et al.*, 2014b].

2.2. Sampling and Measurements

2.2.1. Cruise Sampling

Ten short (1–2 days) cruises (Table 1) were conducted on the R/V *Tioga* to sample water-column carbonate chemistry and pteropod distribution from May 2013 to July 2015 at a series of 6 stations in Wilkinson Basin
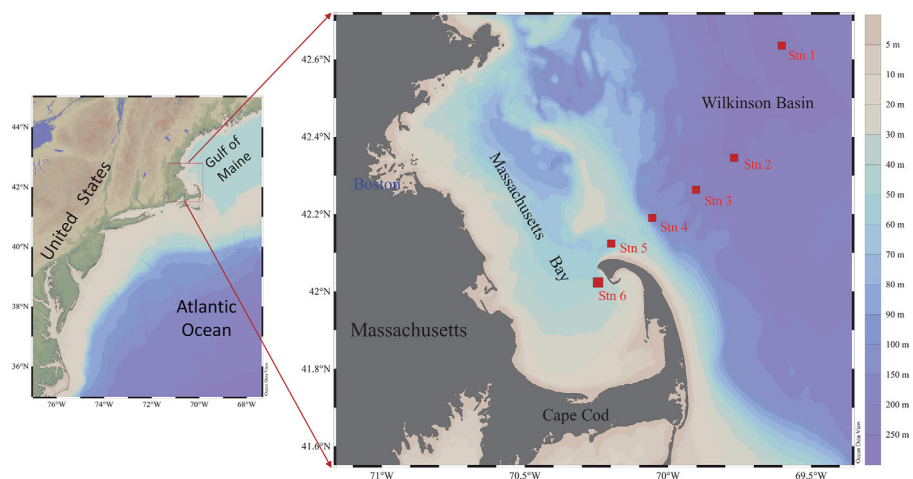

Figure 1. Study area with hydrographic sampling stations (Stations 1–6) in and near Wilkinson Basin in the western Gulf of Maine. Insert, Northeast coast of the United States.

Table 1. Summary of the Research Cruises and Sampled Stations

Cruise Time	May 2013	Aug 2013	Oct 2013	Jan 2014	Apr 2014	Aug 2014	Nov 2014	Apr 2015	May 2015	Jul 2015
Stations	1, 2, 3	1, 2, 3	1, 2, 3	2, 3	2, 3	2, 4	2, 3	2–6	2–6	2–6

and nearby areas (Figure 1). The first seven cruises (2013–2014; Table 1) focused on capturing seasonal variation and occupied at least two stations (Stations 1–4; Figure 1). Station 2 is a deep-basin station (water depth > 250 m) that was always sampled during each cruise. A shallow station (Station 3 or 4) located in the southwest portion of Wilkinson Basin along the flank of Stellwagen Bank was also sampled regularly. Station 1 is another deep station in Wilkinson Basin that was also previously occupied during the two Gulf of Mexico and East Coast Carbon Cruises (GOMECC 1 and 2) in August 2007 and 2012, respectively [*Wang et al.*, 2013; *Wanninkhof et al.*, 2015]. The latter three cruises in 2015 sampled a cross-sectional transect from Station 2 to Station 6 in the southwest of Wilkinson Basin in April–July to study the spring-summer transition (Table 1).

At each station, a 12 position, 5 L bottle Rosette-Niskin package equipped with a Conductivity-Temperature-Depth sensor (CTD, Seabird SBE 911plus) and a SeaTech Chelsea transmissometer was deployed to collect discrete seawater samples for analysis of DIC and total alkalinity (TA). For all cruises, vertical resolution of water sampling was 10–20 m for the upper 100 m and 20–50 m for water depths greater than 100 m. During each cruise, with the exception of May 2015, tows were conducted at Station 2 with a standard 1/4 m^2 Multiple Opening/Closing Net and Environmental Sensing System (MOCNESS) [*Wiebe et al.*, 1985] equipped with 9 nets of 150 μm mesh along with a flowmeter and pressure, temperature, and conductivity sensors to determine the vertical distribution and abundance of pteropods.

2.2.2. Measurements of Carbonate Chemistry

DIC and TA samples were collected in 250 ml Pyrex borosilicate bottles after being filtered with a 0.45 μm in-line capsule filter (Farrwest Environmental Supply, Texas). Each sample was poisoned with 100 μL of a saturated mercuric chloride solution for preservation [*Dickson et al.*, 2007] and sealed with a ground-glass stopper coated with APIEZON®-L grease and secured with a rubber band applied to the bottle top.

DIC samples were measured using an Apollo SciTech DIC auto-analyzer (Model AS-C3) based on nondispersive infrared (NDIR) detection. The sample is acidified with a 10% phosphoric acid in 10% sodium chloride solution, and CO_2 is extracted by purging high purity nitrogen gas, and measured by a LI-COR® 7000 infrared analyzer. Certified Reference Material (CRM) from Dr. A. Dickson at Scripps Institution of Oceanography was used to calibrate the DIC auto-analyzer at least once daily. In addition, CRM was measured as a sample every few hours to gauge and correct any potential drift. The precision and accuracy of the instrument was $\sim \pm 2.0$ μmol kg^{-1}.

TA was titrated with an Apollo SciTech alkalinity auto-titrator (Model AS-ALK2), a Ross combination pH electrode and a pH meter (ORION 3 Star) based on a modified Gran titration [*Wang and Cai*, 2004]. The concentration of hydrochloric acid was calibrated every day using CRMs. The CRMs were also measured as samples every few hours to correct any potential small drift. The accuracy and precision of the instrument was $\sim \pm 2.0$ μmol kg^{-1}. Aragonite saturation state (Ω-Ar) and other carbonate system parameters were calculated using the CO2SYS program by *Pierrot et al.* [2006] with constants from *Mehrbach* [1973] as refit by *Dickson and Millero* [1987].

2.2.3. Pteropod Abundance

Daytime oblique tows, each sampling eight depth intervals on the up cast, were conducted with the MOCNESS at Station 2 during each cruise, with the exception of May 2015. The upper five nets consistently targeted depths of 0–25, 25–50, 50–75, 75–100, and 100–150 m. The depth intervals for the bottom three nets were chosen adaptively during each cruise based on profiles from the transmissometer on the CTD to ensure that the two deepest nets sampled exclusively in the benthic nepheloid layer. The BNL at Station 2 displayed features typical of most of the gulf BNLs [*Pilskaln et al.*, 2014b] with the top of the BNL located at the base of the mid-depth particle minimum zone and where a significant slope change in turbidity begins; a mid-BNL region in which turbidity and attenuation increases substantially with depth; and the lower BNL close to the seafloor where beam attenuation and turbidity are maximal. The protocol was to sample with the deepest net from the maximum depth attained ($\sim$ 5–10 m from the bottom) up to the base of where the turbidity slope began to change significantly; the next net sampled through the region of greatest

turbidity slope change to the top of the BNL. The third net sampled from the top of the BNL up to a depth of 150 m. Upon recovery net contents were preserved in 70% ethanol, a concentration chosen to be high enough to allow DNA preservation but low enough to avoid shell damage (i.e., cracking). All samples had the ethanol replaced with fresh 70% ethanol ~24 h after sampling.

Samples were sorted under microscope and *L. retroversa* identified, dividing large samples into quantitative splits as necessary using a Folsom splitter. This species grows continuously throughout its life and was enumerated in size categories of <1 mm (chosen to correspond to recently spawned early life stages and juveniles) and >1 mm (adults). Small (<0.5 mm) individuals of other thecosomatous pteropod species were occasionally present but at very low abundances; these were not identified to species and are not considered further in this study.

2.3. Sensitivity Analysis of Aragonite Saturation States

Processes and factors that affect aragonite saturation states mostly include photosynthesis, respiration (i.e., remineralization), $CaCO_3$ dissolution-calcification, temperature (t), salinity (S), physical mixing, and CO_2 air-sea exchange. Among these factors and processes, photosynthesis-respiration, dissolution-calcification, and mixing would change DIC and TA in different ways, thus affecting Ω-Ar; air-sea exchange affects Ω-Ar only through changes in DIC; changes in t alone will not change DIC and TA, but will affect carbonic acid dissociation equilibria, thus changing speciation of the CO_2 system (i.e., CO_3^{2-}) and Ω-Ar; salinity change will affect seawater Ca^{2+} concentration and speciation of the CO_2 system as well. The effect of physical mixing, including evaporation and precipitation, is usually small since DIC and TA tend to increase or decrease proportionally during mixing, and their effects on Ω-Ar would likely cancel each other. Air-sea exchange has a very limited effect on Ω-Ar in this study. For example, DIC would only change a few $\mu mol\ kg^{-1}$ in the surface layer (60 m) over the 3 month period in the study region, which only translates to a <0.03 change in Ω-Ar.

To examine the relative contribution of each of these factors in the water column seasonally, a sensitivity analysis was conducted of changes in Ω-Ar over time at the most sampled station, Station 2 (water depth about 260 m), representative of the deep portions of Wilkinson Basin (Figure 1). In this analysis, the water column was divided into three layers: 0 – 60 m, 60 – 160 m, and >160 m, representing near surface, mid-depth, and near bottom conditions. For each depth layer, cruise mean (subscript "c") values of aragonite saturation state ($\overline{\Omega_c}$) were first calculated based on cruise means of t, S, DIC, TA, and pressure (P) at that particular depth layer (subscript "d") using the CO2SYS program:

$$\overline{(\Omega_c)_d} = \Omega\left(\bar{t}_c, \bar{S}_c, \overline{DIC}_c, \overline{TA}_c\right)_d \tag{1}$$

The overall mean Ω-Ar for each depth range, $\overline{(\Omega_a)_d}$, was then calculated from the cruise means. The total deviation of Ω-Ar from the overall mean at a given depth layer for a particular cruise is then given by:

$$(\Delta\Omega_c)_d = \overline{(\Omega_c)_d} - \overline{(\Omega_a)_d} \tag{2}$$

Changes in Ω-Ar over individual changes of DIC, TA, S, and t (i.e., ∂Ω/∂DIC, ∂Ω/∂TA, ∂Ω/∂S and ∂Ω/∂t) are not constant (i.e., are nonlinear) under different seawater conditions. However, if the variability of these parameters is relatively small, the effects of the nonlinearity become insignificant. Under such a condition, $(\Delta\Omega_c)_d$ can be linearly calculated as the sum of individual deviations of Ω-Ar from the overall mean due to changes of t, S, biogeochemical changes of DIC and TA (i.e., photosynthesis-respiration and $CaCO_3$ dissolution-calcification), other minor factors (mixing and air-sea exchange), and error (ε) respectively:

$$(\Delta\Omega_c)_d = (\Delta\Omega_c)_d^t + (\Delta\Omega_c)_d^S + (\Delta\Omega_c)_d^{enDIC} + (\Delta\Omega_c)_d^{enTA} + (\Delta\Omega_c)_d^m + \varepsilon \tag{3}$$

$(\Delta\Omega_c)_d^t$ represents the deviation of Ω-Ar from the overall mean for a given cruise and depth layer solely due to temperature changes. It is calculated by holding three of the four parameters in equation (1) at their overall means and only allowing t to change from cruise to cruise:

$$(\Delta\Omega_c)_d^t = \Omega\left(t_c, \bar{S}_c, \overline{DIC}_c, \overline{TA}_c\right)_d - \overline{(\Omega_a)_d} \tag{4}$$

The Ω-Ar deviation solely due to salinity changes from cruise to cruise at a given depth range, $(\Delta\Omega_c)_d^S$, can be calculated similarly:

$$\left(\Delta\Omega_c\right)_d^S = \Omega\left(\bar{t}_c, S_c, \overline{DIC_c}, \overline{TA_c}\right)_d - \overline{\left(\Omega_a\right)_d} \tag{5}$$

Note that $\left(\Delta\Omega_c\right)_d^S$ only reflects changes resulting from salinity effects on CO_2 speciation and Ca^{2+}, and does not include mixing effects. As biogeochemical activities and mixing all can change DIC and TA, we separate the two types of effects by using salinity normalized DIC (enDIC) and TA (enTA) with the consideration of nonzero end-members (i.e., freshwater end-member) [*Friis et al.*, 2003]:

$$enDIC = \left(DIC_{spl} - DIC_{S=0}\right)/S \times S_{ref} + DIC_{S=0}, \tag{6}$$

where DIC_{spl} is the DIC concentration measured in the sample; $DIC_{S=0}$ is the DIC concentration of the freshwater end-member, determined in section 3.1; S is the salinity of the sample; and S_{ref} is the reference salinity ($S_{ref} = \overline{\left(S_c\right)_d}$ in this case). Salinity normalized TA (enTA) can be defined similarly:

$$enTA = \left(TA_{spl} - TA_{S=0}\right)/S \times S_{ref} + TA_{S=0} \tag{7}$$

Essentially, equations (6) and (7) remove mixing effects from measured DIC and TA by normalizing them to a given (reference) salinity. The deviation of Ω-Ar from the overall mean for a given cruise and depth layer solely due to biogeochemical changes of DIC, $\left(\Delta\Omega_c\right)_d^{enDIC}$, can be calculated by:

$$\left(\Delta\Omega_c\right)_d^{enDIC} = \Omega\left(\bar{t}_c, \bar{S}_c, enDIC_c, \overline{TA_c}\right)_d - \overline{\left(\Omega_a\right)_d} \tag{8}$$

Similarly, we can define the deviation of Ω-Ar solely due to biogeochemical changes of TA:

$$\left(\Delta\Omega_c\right)_d^{enTA} = \Omega\left(\bar{t}_c, \bar{S}_c, \overline{DIC_c}, enTA_c\right)_d - \overline{\left(\Omega_a\right)_d} \tag{9}$$

Lastly, $\left(\Delta\Omega_c\right)_d^m$ represents the deviation of Ω-Ar due to other minor factors (e.g., mixing and air-sea exchange). The term ε includes cumulative errors (e.g., nonlinear effect) of this analysis. $\left(\Delta\Omega_c\right)_d^m$ and ε are defined as the residual between $\left(\Delta\Omega_c\right)_d$ and the sum of $\left(\Delta\Omega_c\right)_d^t$, $\left(\Delta\Omega_c\right)_d^S$, $\left(\Delta\Omega_c\right)_d^{enDIC}$, and $\left(\Delta\Omega_c\right)_d^{enTA}$.

For the maximum DIC deviation of $\sim$60 μmol kg^{-1} that occurred in the surface layer, the change in $\partial\Omega/\partial DIC$ [$\Delta(\partial\Omega/\partial DIC)$] or the nonlinear effect by only allowing DIC to change at a time, is rather small ($\sim$0.0006 in Ω-Ar) if all other parameters are kept at the annual means. This effect is $\sim$0.0003 for $\Delta(\partial\Omega/\partial TA)$, $\sim$0.0007 for $\Delta(\partial\Omega/\partial t)$, and $\sim$0.0001 for $\Delta(\partial\Omega/\partial S)$ at the surface, with an overall effect likely $<$0.002 in Ω-Ar. At depth, this effect is even smaller due to less variability of all the parameters.

3. Results and Discussion

3.1. Overview

The overall distributions of DIC and TA relative to salinity (Figure 2) are similar to the data collected in the GoME from the two previous summertime studies, GOMECC 1 and 2 [*Wang et al.*, 2013; *Wanninkhof et al.*, 2015], although the data collected from this study covered all four seasons over 2 years. Toward the lower end of the salinity range (S $\leq$ 32.4) and near the surface, the DIC data exhibit an enhanced degree of variability relative to salinity, indicative of upper ocean processes, such as biological activity, low salinity water intrusion, and air-sea exchange (Figure 2a). DIC shows less variability for S $>$ 32.4, which reflects the reduced effects of these biogeochemical and physical processes from the subsurface to near bottom.

The TA-salinity plot (Figure 2b) generally reflects three end-member mixing in the study area. Such a mixing regime has been previously observed [*Cai et al.*, 2010; *Wang et al.*, 2013]. The junction point between the two mixing lines in the TA-S plot is slightly different from the previous study [*Cai et al.*, 2010], with the earlier work showing inflection at S $\sim$ 31.75 in contrast to the S $\sim$ 32.45 of this study. The junction point in this study was selected so that the two TA-S mixing lines have the best linear fit (maximum R^2). Extrapolating the two current mixing lines to S = 0, the freshwater end-members in this study are TA = 190.0 $\pm$ 91.0 and 815.9 $\pm$ 22.9 μmol kg^{-1}, which are comparable to those (75 $\pm$ 291 and 932 $\pm$ 17 μmol kg^{-1}) reported by *Cai et al.* [2010], representative of a local freshwater end-member and an upstream freshwater end-member traceable to the rivers emptying into the Labrador Sea, respectively. This junction point of S $\sim$ 32.45 is consistent with the separation point in the DIC-S plot (Figure 2a), indicating that the surface layer of the western GoME is strongly affected by local physical and biogeochemical processes, while under this layer, the DIC and TA distributions bear some indication of remote influences originated in the Labrador Sea. The
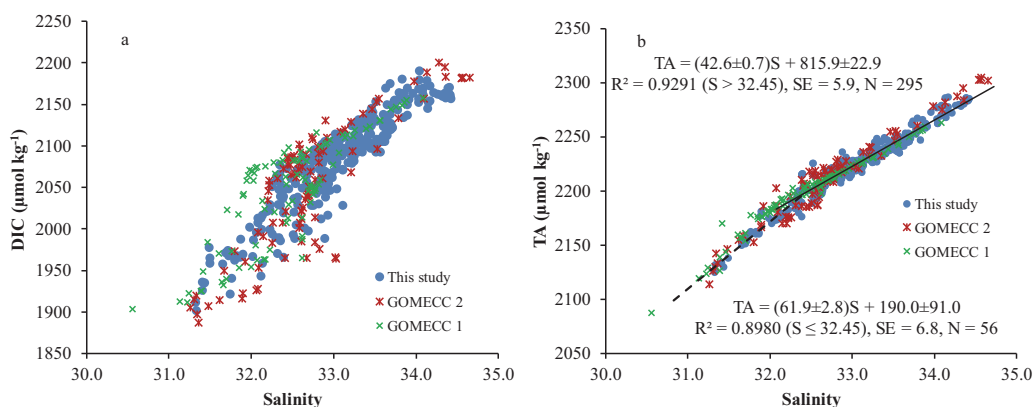
Figure 2. Comparison of DIC and TA measurements from this study and the GOMECC 1 and 2 studies. GOMECC data include all stations in the GoME [*Wang et al*. 2013; *Wanninkhof et al*., 2015]. (a) DIC-salinity distribution; (b) TA-salinity distribution. The solid and dashed lines in Figure 2b are the linear regressions for TA data with S > 32.45 and S ≤ 32.45, respectively.

difference between the current and previous regression lines might reflect slight seasonality in freshwater end-members in our data, while previous data from GOMECC 1 were only obtained in summer. However, such a difference is also rather small and within or close to the respective levels of uncertainty (Figure 2). The two freshwater TA end-member values in Figure 2b were used as both DIC and TA end-members to calculate enTA and enDIC (Equations 6 and 7), assuming that at the freshwater end-member DIC ≈ TA.

3.2. Seasonality of Vertical Distribution

Vertical profiles at Station 2 (Figure 3) exemplify the seasonal progression of physical and biogeochemical processes that affect the marine CO_2 system in Wilkinson Basin. Starting in spring (April and May), stratification began to develop in the upper water column (<60 m). An intensive phytoplankton bloom in May caused a subsurface fluorescence maximum, lowered surface DIC and elevated surface aragonite saturation state and turbidity. DIC increased with depth, while the TA profiles showed small vertical gradients. Ω-Ar decreased significantly with depth, approximately mirroring DIC. In May 2013, Ω-Ar near bottom had a value slightly less than 1, corrosive to aragonite minerals. This undersaturation occurred in the benthic nepheloid layer (Figure 3). High surface production followed by quick sinking and remineralization of surface fresh organic matter at depth at least partially explains this Ω-Ar undersaturation near bottom.

In August, surface stratification was prominent (Figure 3) due to heating and input of low-salinity water (salinity data not shown). Primary production was high. Surface DIC and TA were both relatively low, and increased quickly with depth. Ω-Ar at the surface reached ∼2.6, the highest value observed in this study, and decreased sharply to a value of ∼1.4 at the bottom of the surface layer (∼60 m). It showed limited variation at deeper depths, primarily due to co-increase of DIC and TA. In October, stratification at the surface was relaxed, and primary production was reduced. The profiles of DIC, TA, and Ω-Ar largely followed similar patterns to August, although a thin mixed layer developed in the upper ∼20 m.

By November, the upper 50 m was well mixed, although surface production was still active (Figure 3). The vertical gradients of DIC and TA were relatively small, and still increased with depth. Ω-Ar showed a mid-depth minimum with a value of ∼1.1. In January, surface production was next to none. The water column was well mixed from surface to ∼120 m, below which there were slight increases of DIC and TA followed by a decrease of Ω-Ar to the bottom. Ω-Ar only varied from ∼1.5 at surface to ∼1.3 near bottom. During all sampling periods, the near-bottom waters displayed high turbidity indicating a strong BNL. Winter to spring was the period of greatest near-bottom turbidity observed at Station 2.

In summary, the largest variability of Ω-Ar occurred within the upper 60 m, with highest values in summer and lowest in winter over the study period in the region (Figure 3). This large variability seems to be largely controlled by the stratification-surface production cycle. Ω-Ar at mid-depth (60 – 160 m) showed smaller variation over an annual cycle, with a mean of 1.4 ± 0.2, suggesting less effects of biogeochemical and physical processes at this depth range. Aragonite saturation states were more variable at depths >160 m (compared to the mid-depth), particularly below 200 m (Figure 3). Given the residence time of 1.5 years for
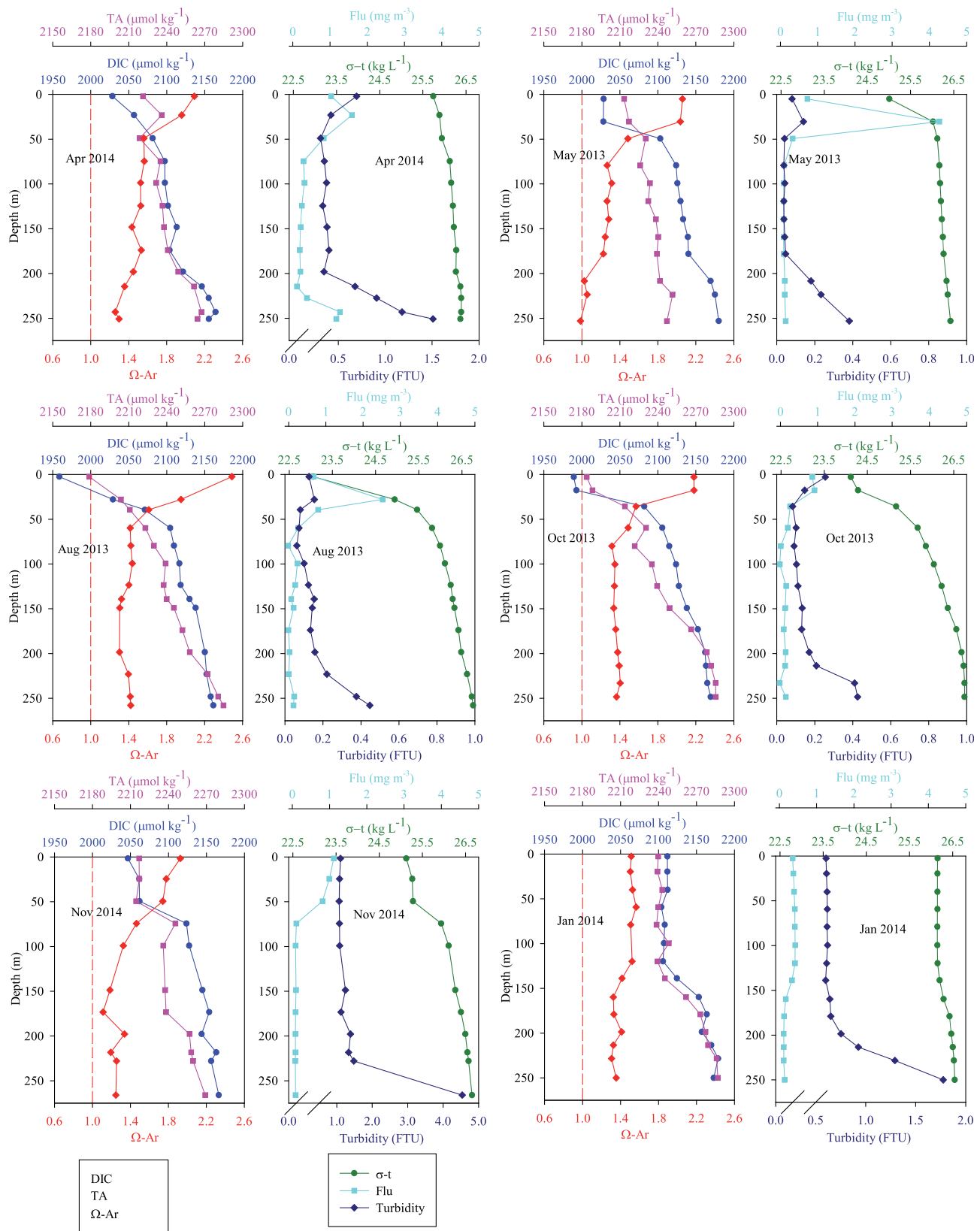
Figure 3. Seasonal vertical profiles of DIC, TA, Ω-Ar, potential density (σ-t), fluorescence (Flu), and turbidity (as FTU) at Station 2 (see Figure 1 for station locations) from 2013 to 2014. The plots are organized by season rather than chronologically for the convenience of discussion.
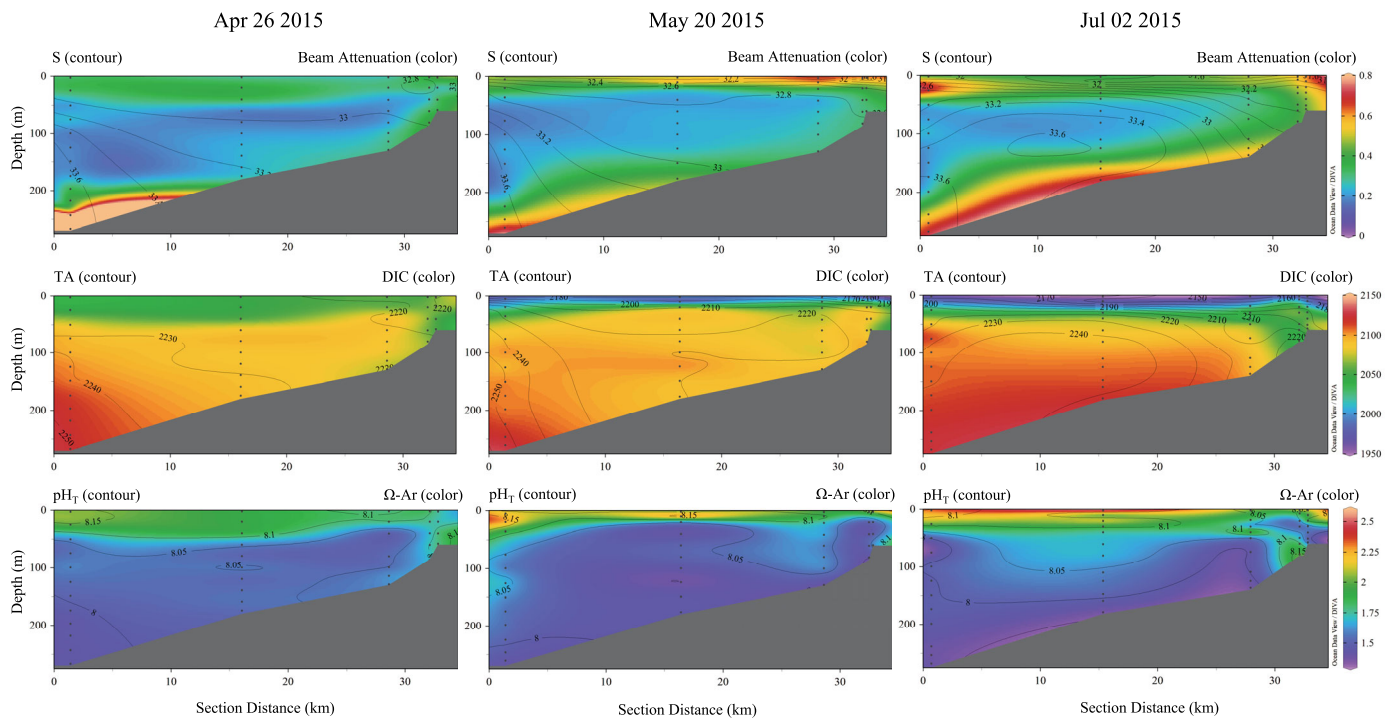
Figure 4. Cross-sectional distributions of S, beam attenuation (m^{-1}), DIC, TA, Ω-Ar, pH$_T$ along the transect between Station 2 (to the left of x-axis) and Station 6 (to the right) during the period of April–July 2015.

deep gulf waters [*Brown and Beardsley*, 1978], the variation in Ω-Ar may be primarily controlled by respiration/remineralization and potential dissolution of aragonite mineral. The relative roles of different controlling processes are examined quantitatively in section 3.4.

3.3. Spring to Summer Transition

During the transition period from spring to summer 2015, the water column near Wilkinson Basin experienced large changes in carbonate chemistry that were associated with both intensive biological activities and physical processes (Figure 4). The three cross-sectional surveys conducted from April to July in 2015 had two purposes: (1) to examine spatial variability of the marine CO$_2$ system and aragonite saturation states from a deep point in Wilkinson Basin up onto the adjacent Stellwagen Bank during a major transition period of the annual cycle; (2) to investigate potentially profound effects of the spring bloom and other processes on distributions of the marine CO$_2$ system, particularly Ω-Ar.

In late April, stratification started to develop across both the deep and shallow stations of Wilkinson Basin (Figure 4). The surface phytoplankton bloom had started, as shown by elevated near-surface beam attenuation in all sampled stations. The BNL was clearly evident below ∼225 m at the deepest station (Station 2). At the shallow nearshore station, moderate turbidity was observed throughout the water column, probably due to shallow mixing. Increased DIC (>2100 μmol kg^{-1}) and TA (>2240 μmol kg^{-1}) water was found at depths >150 m at Station 2, which corresponds to salinity >33.4, pH < 8.0 and Ω-Ar < 1.5. At other stations, vertical distributions of DIC, TA, Ω-Ar, and pH$_T$ showed small gradients.

In late May, the surface phytoplankton bloom had intensified, and was confined to the upper 20–30 m (Figure 4). Stratification had developed with very low salinity (<32.6) water observed in the surface layer. Low salinity water also occupied much of subsurface regions, suggesting intrusion of low salinity water into the area. The BNL also expanded upslope relative to April, from Station 2 to the next deepest station. These changes from April were accompanied by a slight increase of DIC concentration in subsurface water but a decrease of ∼100 μmol kg^{-1} at the surface. TA decreased significantly at the surface, but showed limited changes at depth from April. Tracking the changes in DIC concentration, Ω-Ar and pH$_T$ generally increased at the surface but decreased at depth.

By early July, low salinity water occupied the surface layer at all stations. At the two shallowest stations, the entire water column was occupied with low salinity water (<32.6). Since there is no direct river input to the study area, this low salinity surface water likely originated from river inputs north of the study area, including the Merrimack River and others [Hunt et al., 2011; Salisbury et al., 2009], and was transported to the study region via the Western Maine Coast Current [Jiang et al., 2011]. Precipitation might also contribute to the salinity decrease, although no major weather events occurred before or after the sampling period. On the other hand, high salinity (>33.4) subsurface water was also significantly expanded. Beam attenuation at the surface was further elevated from late May reflecting summer phytoplankton growth, and the BNL was also well developed across all sampling stations. Both DIC and TA were further reduced near the surface, while at depth their concentrations significantly increased from their late May values. The net result of these DIC and TA changes was a further increase of Ω-Ar and pH_T at surface, but large decreases at depth. Ω-Ar and pH_T values in bottom waters were <1.3 and <7.9, respectively. Water intrusion (transport) from the north may at least partially explain these observed changes, although biology likely played an important role as well.

The spring-summer transition has important effects on the distributions of the carbonate system in the water column (Figure 4). Given the generally low Ω-Ar values in subsurface water in the region, two important questions are: (1) What are the dominant factors or process controlling the Ω-Ar distribution during the transition season? and (2) Does aragonite dissolution occur during the high production season in the GoME, when high rates of remineralization are expected at depth, increasing CO_2 and lowering pH and Ω-Ar? Figure 4 suggests that both biological activities and physical mixing may play roles of controlling the CO_2 parameters during the spring-summer transition. To remove physical mixing effects, enDIC and enTA were calculated based on equations (6) and (7) to isolate changes due to nonconservative processes and corresponding changes of Ω-Ar between the three consecutive cruises from April to July 2015 (Figure 5).

After removing the effects of mixing, the changes in Ω-Ar ($\Delta\Omega$) calculated between each pair of consecutive cruises from April to July 2015 mostly followed changes in enDIC (ΔenDIC) expected based on photosynthesis and respiration/remineralization alone (Figure 5a). This is a strong indication that photosynthesis and respiration were the primary biogeochemical drivers of the observed variability in Ω-Ar during the transition. These two drivers caused a change in Ω-Ar on the order of ~1.2 (~-0.6 to 0.6 in $\Delta\Omega$), which covered almost the entire range of Ω-Ar during this period (Figure 4). The data points in Figure 5a representing changes between the April and May 2015 cruises are more evenly spread across the photosynthesis versus respiration side (i.e., negative and positive sides) of the theoretical curve. This suggests that the net effects of biogeochemical
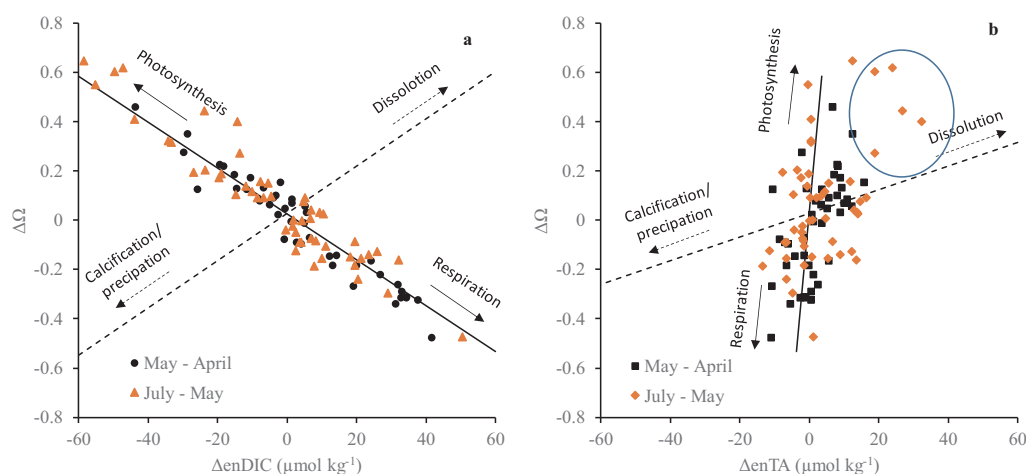

Figure 5. Changes of aragonite saturation states ($\Delta\Omega$) between three consecutive cruises from April – July 2015 as a function of (a) changes in enDIC (ΔenDIC), and (b) changes in enTA (ΔenTA). The data points circled in Figure 5b represent potential alkalinity sources other than photosynthesis-respiration and calcification-dissolution. $\Delta\Omega$, ΔenDIC, and ΔenTA were calculated first by gridding all data for each cruise using the Ocean Data View® Diva method, then by taking differences of each sampling point between two consecutive cruises, May–April and July–May, respectively. Solid black lines are theoretical lines of $\Delta\Omega$ versus ΔenDIC and $\Delta\Omega$ versus ΔenTA expected if only photosynthesis and respiration/remineralization occur. Dashed lines are theoretical lines if only calcification and dissolution of $CaCO_3$ occur. These were calculated by using mean values of enDIC and enTA across all three cruises, and Redfield ratios (ΔenDIC : ΔenTA $= -106$: $+16$) for photosynthesis-respiration and the ratio ΔenDIC : ΔenTA $= 1: 2$ for calcification-dissolution.

processes, mainly photosynthesis and respiration/remineralization, may largely balance each other and that net ecosystem production (NEP) of the system may be close to zero during the period of April–May. Comparing May and July, more data points are shifted toward the photosynthesis side of the curve (Figure 5a), which suggests that the system may be shifted to be more autotrophic (NEP > 0). Such a conclusion is consistent with more intensive primary production associated with the spring bloom at surface during this period. Since $\Delta\Omega$ reflects the net changes of all biogeochemical and physical processes, but follows the photosynthesis-respiration line closely (Figure 5), physical processes did not have a detectible effect on Ω-Ar as described in section 2.3, although there was low salinity water entering the study area during the transition (Figure 4).

Changes in Ω-Ar also mostly follow the theoretical changes in enTA expected for photosynthesis-respiration, strengthening the conclusion described above. The apparent scatter of the data might be because changes in enTA due to photosynthesis-respiration were inherently small (ΔenDIC : ΔenTA = -106 : $+16$) [*Goldman and Brewer*, 1980; *Wolf-Gladrow et al*., 2007], which may be close to the uncertainty of the analysis. Using differences in duplicate measurements of DIC and TA (0.9 ± 6.2, N = 24 and 1.0 ± 5.2, N = 29, respectively) as the error margin, it translates to ~3% uncertainty in Ω-Ar (~$\pm 0.03 – 0.06$ in this study) [*Riebesell et al*., 2010]. The 4–5 data points (circled in Figure 5b) away from the theoretical photosynthesis-respiration line may indicate other sources of alkalinity in the region. These samples were from the subsurface and bottom water (20 – 78 m) of the most nearshore stations (Station 5 and 6). ΔenTA of these data ranged from $+18 – +32$ μmol kg^{-1} between May and July, with corresponding ΔenDIC of -14 to -50 μmol kg^{-1}. Photosynthesis-respiration does not seem to be sufficient to explain the relatively large increase of enTA at these locations between May and July and other biogeochemical processes that generate alkalinity are thus likely at play. Given the shallowness of the location, inputs of products from anaerobic respiration in sediments, particularly denitrification, is one possible explanation [*Fennel*, 2010]. CaCO$_3$ dissolution might also be a candidate as those data points are approaching the calcification-dissolution line in Figure 5b. Although subsurface aragonite saturation states were above 1 (~1.4) at those stations, dissolution might occur in sediments, creating an alkalinity source to the water column.

3.4. Pteropod Abundance

Patterns in thecosome pteropod distribution and abundance were examined to gain initial insight into the influence of seasonal variability in GoME carbonate chemistry on pteropods and vice versa. Carbonate chemistry and pteropod distribution at Station 2 (Figure 1) were both sampled throughout the water column during all cruises except May 2015. Numerical densities were greatest overall in net samples made in the upper 50 m of the water column (ranging from 0 to 154.1 individuals m^{-3}) and lower at mid-depths (50–150 m; range 0–0.6 individuals m^{-3}). Pteropods were absent at deeper depths, within and immediately above the BNL, with the exception of July 2015 when low numbers of animals were also present within and just above the BNL (0.06–0.1 inds m^{-3}).

Depth-integrated densities at Station 2 showed strong patterns of seasonal variability. Small individuals (< 1 mm) varied by orders of magnitude in abundance over the 2 years of sampling (Figure 6). Examinations of seasonal changes in size distributions and gonad development have suggested *L. retroversa* spawning peaks in the GoME in May, but with active reproduction continuing into the fall [*Hsiao*, 1939]. A recent laboratory study of *L. retroversa* reproductive and developmental biology also found that this species is capable of spawning multiple times per year, and suggest that, in this region, individuals likely live ~6 months [*Thabet et al*., 2015]. Abundances of small individuals were very high in May 2013 and April–June 2015, indicative of a strong springtime spawning event, presumably associated with the spring bloom. Moderate abundances were also sampled in summer 2013 and summer/fall 2014, consistent with continued spawning after the spring bloom. Abundances in fall 2013 and May 2014 were comparatively much lower, however. The GoME is a dynamic system and *L. retroversa* is thought to be advected in from outside the Gulf and then transported through it following the overall cyclonic flow over the course of more than one generation [*Redfield*, 1939]; the variability in abundance might reflect inter-generational variability in recruitment success and input from upstream sources. It might also reflect spatial patchiness.

Large pteropods (> 1 mm) were much less abundant and generally showed less variability between cruises (Figure 6), with the exceptions of August 2013/2014 and April 2014, when no large individuals were captured, and July 2015, when abundance was several fold higher than at other times. These times may again be associated with patterns in the pteropod reproductive cycle in the region. The absences may reflect the
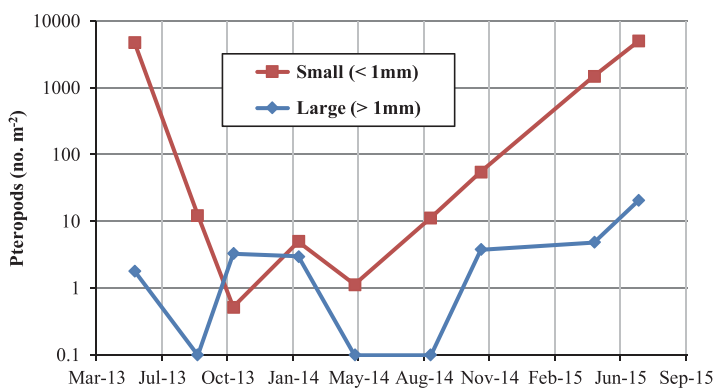
Figure 6. Abundance of small (< 1 mm; red) and large (> 1 mm; blue) *Limacina retroversa* sampled at Station 2 during each cruise. Numerical densities from the eight MOCNESS nets were vertically integrated over the full sampled portion of the water column (to maximum depths of ca. 250–260 m, i.e., within 5–10 m of the bottom) and are expressed as number (no.) individuals m^{-2}. Note that the abundance data are log$_{10}$-transformed and values of zero pteropods are plotted here as 0.1.

senescence and death of large reproductive adults after spring and summertime reproductive events, while the peak in July may be a consequence of the cohort spawned in spring reaching reproductive maturity in advance of the second seasonal spawn. These anomalies may again also relate to patchiness and advection of cohorts of animals through the region.

For pteropods > 1 mm in size, there was generally a positive relationship between depth-integrated abundance and mean aragonite saturation state of the water column at Station 2 (R=0.317; Figure 7a), with the exceptions of the absences in August 2013/2014 and April 2014 and the anomalously high abundance in July 2015. Excluding these data points in order to assess the relationship between carbonate chemistry and living pteropods, when present, the rest of the data showed a linear correlation between mean Ω-Ar of water column and large pteropod abundance, though not quite significant (Pearson Correlation, two-tail; R=0.782, p=0.118).

Given the outliers, small sample size, and uncertainty in abundance estimates due to spatial and temporal patchiness, this relationship should be further validated in the future, but the possible correlation does raise interesting questions concerning the relationship between Ω-Ar and pteropod distribution in the GoME. The positive association may indicate conditions that are energetically more favorable for pteropod calcification, and hence greater scope for growth and competitive success, as Ω-Ar increases [*Waldbusser et al.*, 2015], although the effects of Ω-Ar on pteropods, as for other calcifying organisms, for Ω-Ar > 1 may not be straightforward [*Bednarsek et al.*, 2014; *Cyronak et al.*, 2016]. It is also possible that the positive relationship is simply spurious. Alternatively, it may represent an indirect association between pteropod abundance and
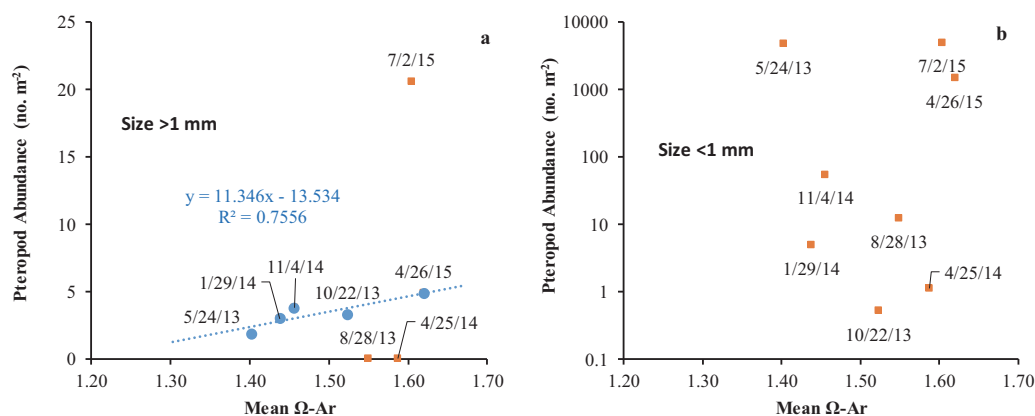

Figure 7. Pteropod abundance (vertically integrated over the full sampled portion of the water column) as a function of mean aragonite saturation states (Ω-Ar) in the water column at Station 2. (a) Pteropods of size > 1 mm; (b) Size < 1 mm. The linear best-fit line in Figure 7a only includes the data in blue (see text for details).

Ω-Ar mediated by synchrony between the pteropod life cycle and senescence after reproductive events with times of high productivity (i.e., spring and fall blooms) at which time enhanced DIC serves to decrease Ω-Ar. Related to this notion, it is possible that the life cycle of *L. retroversa* in the region is optimized such that large reproductive adults are most abundant during periods when their larvae have a better chance of passing the initial calcification bottleneck [*Thabet et al.*, 2015; *Waldbusser et al.*, 2013, 2015], and this causes successful cohorts to appear in large numbers during periods when Ω-Ar is high (as well as food abundant). If so, it will become useful to consider how the predicted changes in saturation state might influence their future spawning success.

In contrast, there was no apparent relationship between pteropod abundance and Ω-Ar for pteropods <1 mm in size (Figure 7b), suggesting that other factors, likely associated with adult reproductive success and predator-prey dynamics determine juvenile cohort abundances. As there remains some debate as to which carbonate chemistry parameter is the most physiologically meaningful for calcifying organisms [*Cyronak and Eyre*, 2016; *Cyronak et al.*, 2016; *Waldbusser et al.*, 2015], we regressed abundances of both size classes with pH and the ratio of $[H^+]$ to $[HCO_3^-]$, in addition to Ω-Ar, finding that at current conditions of the study region, pH and the ratio of $[H^+]$ to $[HCO_3^-]$ did not strongly correlate with either size class.

3.5. Seasonal Controls of Aragonite Saturation

On a seasonal scale, Figure 3 showed large variability in water-column carbonate chemistry corresponding to physical and biogeochemical changes. The goal of this section is to examine the individual factors that may control the seasonal variability of aragonite saturation in different depth layers of the water column and how they interact to determine the overall seasonal distribution of aragonite saturation states in the western GoME. Such knowledge is critical in developing a mechanistic understanding and models to study future changes in seawater chemistry and their impacts in the region. Sensitivity analysis for aragonite saturation state (see section 2.3) was therefore applied to the data collected at Station 2 in three depth layers over the 2 year sampling period.

Surprisingly, the large variability observed in Ω-Ar in the surface layer (<60 m) did not show a clear seasonal pattern over the 2 year period (Figure 8a). The largest negative deviation of Ω-Ar ($\Delta\Omega_c$) from the mean occurred in January 2014, corresponding to an almost uniform water column and ventilation of deep water, which contained high DIC (CO_2), likely resulting from cumulative effects of respiration and remineralization. The largest positive excursion in $\Delta\Omega_c$ occurred in late May to early July 2015, the transition from spring to summer, when intensive surface production occurred (Figure 4). At other times, $\Delta\Omega_c$ showed less deviation from the mean. $\Delta\Omega_c$ more closely followed $\Delta\Omega^{enDIC}$, indicating that most deviations of Ω-Ar were solely due to biogeochemcial changes in DIC. Next to $\Delta\Omega^{enDIC}$, $\Delta\Omega^{enTA}$ mostly exhibited smaller, but significant influences on $\Delta\Omega_c$, except in January and April 2014 when $\Delta\Omega^{enTA}$ and $\Delta\Omega^{enDIC}$ were both significant, but in opposite signs. The time-series of $\Delta\Omega^{enDIC}$ and $\Delta\Omega^{enTA}$ were thus mostly consistent with the conclusion that photosynthesis and respiration were the major drivers of $\Delta\Omega_c$ at the surface. In contrast to $\Delta\Omega^{enDIC}$, $\Delta\Omega^{enTA}$ showed a small, but clear seasonal pattern at the surface, with more positive effects on Ω-Ar in spring and more negative effects in fall (Figure 8a). This is consistent with the balance between photosynthesis and respiration at the surface, with net production in spring and net respiration in fall. The observation that $\Delta\Omega^{enDIC}$ displayed less of a seasonal pattern than $\Delta\Omega^{enTA}$ may reflect the greater sensitivity of DIC to most biogeochemical processes as compared to TA, with the exception of $CaCO_3$ dissolution and calcification. $CaCO_3$ dissolution is unlikely to affect Ω-Ar near surface as its values were relatively high (mean 1.8 ± 0.2). However, calcification might play a role in the surface layer. For example, in addition to net respiration, the relatively large negative value of $\Delta\Omega^{enTA}$ in fall might be a sign of calcification. Both effects of temperature and salinity ($\Delta\Omega^t$ and $\Delta\Omega^S$) were relatively insignificant over the 2 year period (Figure 8a). Since other minor effects ($\Delta\Omega^m$, including mixing and air-sea exchange) are likely small, $\Delta\Omega^m + \varepsilon$ in Figure 8a mostly reflects the cumulative error, ε, for this analysis (section 2.3). At the surface layer, this error was relatively consistent ($\sim$0.1) over the study period (Figure 8a). As such, ε does not likely affect previous conclusions for the surface layer. As the nonlinear error is small (section 2.3), ε might include other errors. One likely error may be from calculation of enDIC and enTA, namely the inaccuracy of defining the two different freshwater endmembers (Figure 2), which can cause an offset in enDIC and enTA, thus an offset in Ω-Ar. However, such an offset will not change the pattern of any variation discussed here. This error may decrease with increase of depth (and S) (see below) as reflected in less variability of TA in subsurface and near-bottom water (Figure 2).
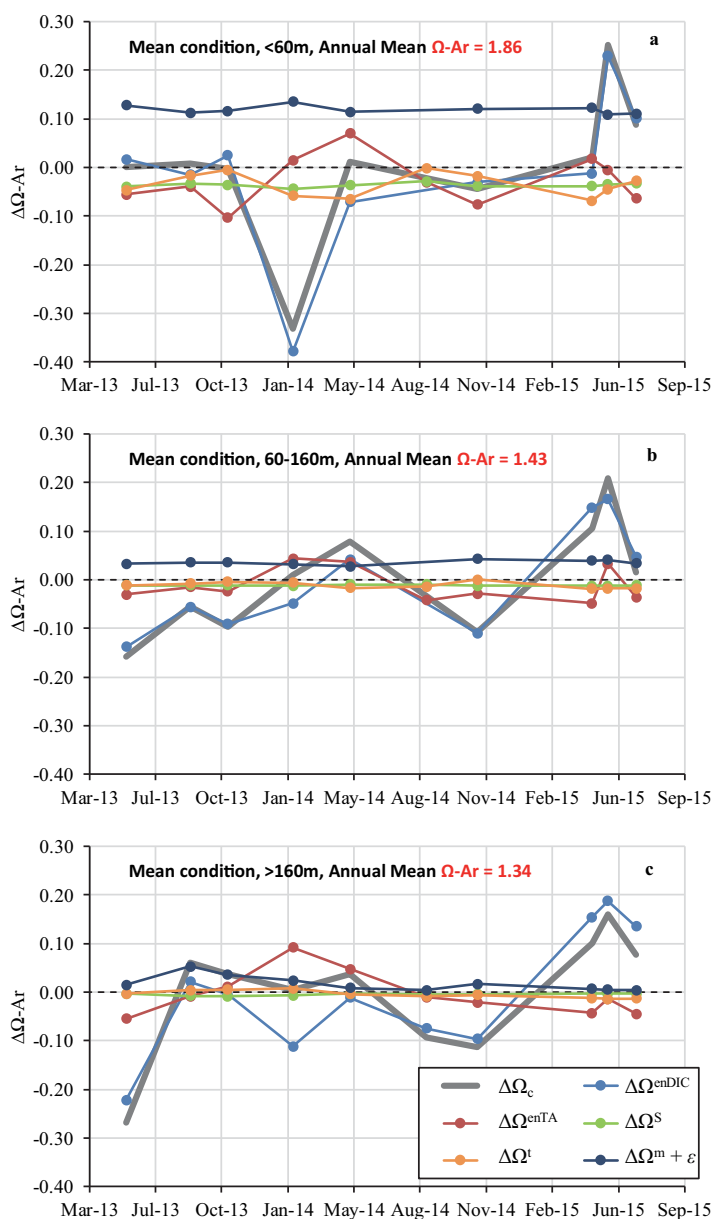
Figure 8. Sensitivity of seasonal deviations of aragonite saturation state from its overall mean ($\Delta\Omega_c$) due to seasonal changes of enDIC ($\Delta\Omega^{enDIC}$), enTA ($\Delta\Omega^{enTA}$), S ($\Delta\Omega^S$), temperature ($\Delta\Omega^t$) and other minor processes plus error ($\Delta\Omega^m + \varepsilon$) in three depth layers at Station 2. (a) <60 m; (b) 60–160 m; (c) >160 m.

$\Delta\Omega_c$ at mid-depths (60–160 m) showed a seasonal pattern, with maxima occurring in spring and minima in late fall and winter (Figure 8b). The exception to this pattern was May 2013 when a large deficit in $\Delta\Omega_c$ was evident in the mid-depth layer, at which time $\Delta\Omega_c$ at the surface was close to the annual mean. $\Delta\Omega^{enDIC}$ again was the primary driver of $\Delta\Omega_c$, while $\Delta\Omega^{enTA}$ played a minor role. As photosynthesis was not expected to have an effect at this depth, $\Delta\Omega^{enDIC}$ and $\Delta\Omega^{enTA}$ mostly reflect the degree of accumulation of respiration/remineralization products in this depth layer. Due to the limited effects from $\Delta\Omega^{enTA}$, $CaCO_3$ dissolution and calcification were likely insignificant. The large negative deviation in the surface layer in January 2014 was not observed at this depth, consistent with deep water ventilation causing surface decrease of Ω-Ar, but limited effect at depth. From May 2014 onward, $\Delta\Omega_c$ and $\Delta\Omega^{enDIC}$ in this depth range approximately followed that of the surface layer, suggesting a direct linkage between the two layers. The effects of temperature and salinity on Ω-Ar were negligible here ($\Delta\Omega^t$ and $\Delta\Omega^S$ were between −0.02 – +0.02). $\Delta\Omega^m + \varepsilon$ were smaller than the surface layer and also varied little over the study period.

In the bottom layer (>160 m), although there was a certain degree of similarity in the seasonal pattern of $\Delta\Omega_c$ compared to the mid-depth layer, differences were also noticeable from October 2013 to April 2014 (Figure 8c) during which time $\Delta\Omega^{enTA}$ played an important role in shaping $\Delta\Omega_c$ at depth. At other times over the study period, $\Delta\Omega^{enDIC}$ exerted a primary effect on $\Delta\Omega_c$ and $\Delta\Omega^{enTA}$ was secondary at this depth, suggesting that respiration/remineralization was the major driver. Effects of mixing, temperature, salinity, and error were all insignificant in this depth layer, consistent with its relatively stable physical condition year round (Figure 3). However, the relatively large positive influence of $\Delta\Omega^{enTA}$ on $\Delta\Omega_c$ compared to $\Delta\Omega^{enDIC}$ in January and April 2014 suggests that respiration/remineralization alone cannot explain $\Delta\Omega_c$ and instead, calcification-dissolution must have played an enhanced role. For the mean seawater condition experienced in this layer (S = 33.8, t = 6.9°C, TA = 2259 µmol kg^{-1}, DIC = 2145 µmol kg^{-1}), the net effect of respiration/remineralization would be a decrease of Ω-Ar, where ~1 part is due to decrease of TA and ~21 parts due to increase of DIC based on the Redfield Ratio (ΔTA:ΔDIC ~ −16:106) and CO_2 equilibrium calculations. In contrast, $CaCO_3$ dissolution in the same water would cause Ω-Ar to increase, where ~2 parts would be from an increase of TA, but an increase of DIC would reduce that by ~1 part. Although respiration/remineralization likely still exert an influence in January and April 2014, the relative magnitudes of the positive effects of $\Delta\Omega^{enTA}$ (Figure 8c) were an indicator that $CaCO_3$ dissolution also played a role. $CaCO_3$ dissolution could be occurring in the water column, during sediment resuspension, and/or in the upper sediments where alkalinity would be released to the water column. Since pteropod shells are not found in gulf sediments, and only calcitic, planktonic foraminifera are sufficiently preserved [*Keigwin and Pilskaln*, 2015], it may be more plausible that aragonite dissolution occurs in bottom water. The decrease in pteropod abundance from January 2014 to May 2014 (Figure 6) was also consistent with possible aragonite dissolution at depth. Large pteropods were perhaps dying and then sinking of out of the water column, providing a source of aragonite to support this increased role of dissolution in controlling saturation state at this time of year. At other times of year, particularly during times of high productivity, the contributions of pteropod calcification and dissolution to water-column carbonate chemistry is likely overwhelmed by the photosynthesis-respiration/remineralization signal.

Previously collected sediment trap data in Wilkinson Basin (2008–2010) have also indicated that dissolution of pteropod aragonitic shells likely constitutes the major loss of $CaCO_3$ in the water column at depth during late fall and winter in the western GoME [*Hayashi*, 2014]. It should be also noted that trap-measured POC export in the region from 2008 through 2010 consistently displayed greater export through the water column in late fall as compared to the post-spring bloom period [*Hayashi*, 2014; *Pilskaln et al.*, 2014b]. Such evidence supports the hypothesis that remineralization and respiration-driven aragonite dissolution plays an important role in controlling the carbonate chemistry and alkalinity budget in the deep waters of the gulf. Although sediment anaerobic respiration may also release TA to the water column, the highest value of $\Delta\Omega^{enTA}$ in January 2014 was not coincident with the likely timing of high rates of sediment anaerobic respiration which usually occurs in high production seasons. Although Ω-Ar was low overall (1.34 ± 0.13) in the bottom layer, undersaturation was only observed in May 2013 and the water column was slightly oversaturated during January 2014 when dissolution appears to have played a role. Aragonite undersaturation also occurred at Station 1 in August 2012 during the GOMECC 2 [*Wanninkhof et al.*, 2015]. It is unclear if undersaturation of aragonite occurred between any sampling events. It is possible that because aragonite shells are generally in higher abundance from fall to winter compared to the other seasons (based on sediment trap and plankton tow data), the observable effects from dissolution are more pronounced. Further studies are warranted to examine aragonite saturation states in higher spatiotemporal resolution and to address the issue of whether or not aragonite dissolution occurs in situ when Ω-Ar is above 1 in the GoME [*Feely et al.*, 1988].

4. Conclusions and Implications

This study demonstrates that water-column carbonate chemistry in the deep reaches of Wilkinson Basin in the western Gulf of Maine undergoes a seasonal cycle, wherein the water column stratification-overturn cycle, surface primary production/respiration, subsurface respiration/remineralization, and mixing all play important roles at distinct spatial and temporal scales. Aragonite saturation states are sensitive to the

variation of biogeochemical processes, exhibiting a range from slight undersaturation ($\sim$0.9) near the bottom in spring to 2.6 at the surface in summer. Below 100 m in Wilkinson Basin, mean Ω-Ar rarely exceeds 1.5 years round. At depth, especially in the BNL, respiration-remineralization of bloom products sometimes results in seasonal aragonite undersaturation.

Along a cross-section from the deep part of Wilkinson Basin to shallow banks, the water column experienced a transition between April and July 2015 from an approximately production-respiration balanced system to a net autotropic system at surface. At depth, accumulation of remineralization products from sinking surface production increased DIC and decreased TA and Ω-Ar significantly, suggesting surface production and remineralization at depth are tightly coupled in the western GoME during the spring-summer transition. Simultaneously, low-salinity water intrusion during the transition period lowered DIC and TA in surface waters of the deep basin and the effect reached the bottom of the shallow banks. However, photosynthesis and respiration were the primary driving forces changing Ω-Ar during the spring-summer transition. On the shallow banks, benthic anaerobic respiration and $CaCO_3$ dissolution in sediments might also play a role in affecting Ω-Ar near bottom by providing a TA source.

Over the 2 years of sampling, the mean Ω-Ar in the water column showed a positive relationship with the total abundance of large pteropods (>1 mm). There were outliers in this pattern, however, and the patchy nature of pteropod spatial distribution, coupled with temporal variability in abundance associated with the *L. retroversa* reproductive cycle and advection into the GoME from upstream sources, complicate exploration of the linkages between local carbonate chemistry and pteropod abundance. Further investigation into these linkages is warranted to establish whether the correlation observed here is spurious, represents an indirect association between pteropod abundance and Ω-Ar mediated by the seasonal productivity cycle and the impact of DIC on Ω-Ar, or a direct effect of saturation state on the success of pteropod populations in the region. Furthermore, as acidity in the region increases, it will be valuable to determine whether other carbonate parameters (such as pH or the ratio of $[H^+]$ to $[HCO_3^-]$) affect abundance via different physiological mechanisms.

The sensitivity analysis reveals that photosynthesis-respiration at surface and respiration-remineralization at depth in Wilkinson Basin are the primary driving force of Ω-Ar variability in the water column. However, $CaCO_3$ dissolution may occur during the fall-winter period when near bottom Ω-Ar is generally low. Such a conclusion is supported by a decrease in the abundance of large pteropods observed between winter and spring samples as well as previous $CaCO_3$ flux trap measurements in the region. The data suggest that $CaCO_3$ dissolution may occur in the water column (aragonite dissolution with Ω-Ar slightly above 1) and/or sediment (resulting TA is released from sediment to the water column). The former mechanism seems to be more in line with pteropod shell distribution, previous trap measurements and $CaCO_3$ preservation in sediment, although more studies are needed to disentangle the two mechanisms. Physical mixing was generally an insignificant factor controlling Ω-Ar variability at all depths. Changes in temperature and salinity generally displayed limited effects on changes in Ω-Ar throughout water column year round.

The results from this study have significant implications for $CaCO_3$ shell-forming organisms in the GoME ecosystem. The current mean condition of carbonate chemistry in the western GoME is such that Ω-Ar can be expected to decrease by 0.01 for every 1 μmol kg^{-1} increase of DIC (Figure 5), which is approximately the annual rate of CO_2 invasion in open ocean [*Bates et al.*, 2014]. If such a rate represents the CO_2 invasion rate in the GoME and assuming no other changes occur, the mean Ω-Ar of the subsurface and bottom water in Wilkinson Basin (Figure 8) will approach undersaturation with respect to aragonite minerals in 30–40 years. Ω-Ar exhibits a natural variability of $\pm$0.6 units (Figure 5). As such, subsurface and bottom waters in the region will most likely experience consistent seasonal undersaturation of aragonite, and ocean acidification could have negative impacts on the diverse shell-forming plankton and shellfish species in the GoME in the near future. As shown in this study, photosynthesis and respiration are the major driving mechanisms of Ω-Ar variability in the water column. Any biological regime changes in the GoME (e.g., changes in stratification affecting the spring bloom) thus may have significant consequences on the carbonate chemistry. More in-depth studies of changing seawater chemistry and its complex consequences and feedbacks are thus highly recommended.

References

Alin, S. R., et al. (2012), Water chemistry, larval oysters, and ocean acidification in a complex, urbanized estuary (Puget Sound, Washington), *J. Shellfish Res.*, *31*(1), 259–259.

Andersson, A. J., K. L. Yeakel, N. R. Bates, and S. J. de Putron (2014), Partial offsets in ocean acidification from changing coral reef biogeochemistry, *Nat. Clim. Change*, *4*(1), 56–61.

Armstrong, J. L., J. L. Boldt, A. D. Cross, J. H. Moss, N. D. Davis, K. W. Myers, R. V. Walker, D. A. Beauchamp, and L. J. Haldorson (2005), Distribution, size, and interannual, seasonal and diel food habits of northern Gulf of Alaska juvenile pink salmon, *Oncorhynchus gorbuscha*, *Deep Sea Res., Part II*, *52*(1-2), 247–265.

Balch, W. M., D. T. Drapeau, B. C. Bowler, and T. G. Huntington (2012), Step-changes in the physical, chemical and biological characteristics of the Gulf of Maine, as documented by the GNATS time series, *Mar. Ecol. Prog. Ser.*, *450*, 11–35.

Barton, A., et al. (2015), Impacts of coastal acidification on the Pacific Northwest Shellfish Industry and adaptation strategies implemented in response, *Oceanography*, *28*(2), 146–159.

Bates, N. R., Y. M. Astor, M. J. Church, K. Currie, J. E. Dore, M. Gonzalez-Davila, L. Lorenzoni, F. Muller-Karger, J. Olafsson, and J. M. Santana-Casiano (2014), A time-series view of changing surface ocean chemistry due to ocean uptake of anthropogenic CO2 and ocean acidification, *Oceanography*, *27*(1), 126–141.

Bednarsek, N., et al. (2012), Extensive dissolution of live pteropods in the Southern Ocean, *Nat. Geosci.*, *5*(12), 881–885.

Bednarsek, N., G. A. Tarling, D. C. E. Bakker, S. Fielding, and R. A. Feely (2014), Dissolution dominating calcification process in polar pteropods close to the point of aragonite undersaturation, *Plos One*, *9*(10), e109183, doi:10.1371/journal.pone.0109183.

Berelson, W. M., W. M. Balch, R. Najjar, R. A. Feely, C. Sabine, and K. Lee (2007), Relating estimates of CaCO₃ production, export, and dissolution in the water column to measurements of CaCO₃ rain into sediment traps and dissolution on the sea floor: A revised global carbonate budget, *Global Biogeochem. Cycles*, *21*, GB1024, doi: 10.1029/2006GB002803.

Bernard, K. S., and P. W. Froneman (2009), The sub-Antarctic euthecosome pteropod, *Limacina retroversa*: Distribution patterns and trophic role, *Deep Sea Res., Part I*, *56*(4), 582–598.

Bigelow, H. B. (1924), Plankton of the offshore waters of the Gulf of Maine, *Bull. U. S. Bur. Fish.*, *40*, 1–509.

Breitburg, D. L., et al. (2015), And on top of all that. . . coping with ocean acidification in the midst of many stressors, *Oceanography*, *28*(2), 48–61.

Broecker, W. S. (2009), Wally's quest to understand the ocean's CaCO3 cycle, *Annu. Rev. Mar. Sci.*, *1*, 1–18.

Brown, W. S., and R. C. Beardsley (1978), Winter circulation in Western Gulf of Maine. 1. Cooling and water mass formation, *J. Phys. Oceanogr.*, *8*(2), 265–277.

Cai, W. J., X. P. Hu, W. J. Huang, L. Q. Jiang, Y. C. Wang, T. H. Peng, and X. Zhang (2010), Alkalinity distribution in the western North Atlantic Ocean margins, *J. Geophys. Res.*, *115*, C08014, doi:10.1029/2009JC005482.

Cai, W. J., et al. (2011), Acidification of subsurface coastal waters enhanced by eutrophication, *Nat. Geosci.*, *4*(11), 766–770.

Caldeira, K. (2007), Phanerozoic ocean chemistry and anthropogenic ocean acidification, *Geochim. Cosmochim. Acta*, *71*(15), A140–A140.

Comeau, S., R. Jeffree, J. L. Teyssie, and J. P. Gattuso (2010), Response of the Arctic Pteropod Limacina helicina to projected future environmental conditions, *Plos One*, *5*(6), e11362, doi:10.1371/journal.pone.0011362.

Cooley, S. R., and S. C. Doney (2009), Anticipating ocean acidification's economic consequences for commercial fisheries, *Environ Res Lett*, *4*(2), doi:10.1088/1748-9326/4/2/024007.

Cooley, S. R., N. Lucey, H. Kite-Powell, and S. C. Doney (2011), Nutrition and income from molluscs today imply vulnerability to ocean acidification tomorrow, *Fish Fish.*, *13*(2), 182–215, doi:10.1111/j.1467-2979.2011.00424.x.

Cyronak, T., and B. D. Eyre (2016), The synergistic effects of ocean acidification and organic metabolism on calcium carbonate (CaCO3) dissolution in coral reef sediments, *Mar. Chem.*, *183*, 1–12.

Cyronak, T., K. G. Schulz, and P. L. Jokiel (2016), The Omega myth: What really drives lower calcification rates in an acidifying ocean, *ICES J. Mar. Sci.*, *73*(3), 558–562.

Dickson, A. G., and F. Millero (1987), A comparison of the equilibrium constants for the dissociation of carbonic acid in seawater media, *Deep Sea Res., Part A*, *34*, 1733–1743.

Dickson, A. G., C. L. Sabine, and J. R. Christian (2007), *Guide to best practices for ocean CO₂ measurements*, PICES Special Publication 3, 191 pp. North Pacific Marine Science Organization, Sidney, British Columbia, Canada.

Doney, S. C., V. J. Fabry, R. A. Feely, and J. A. Kleypas (2009), Ocean Acidification: The other CO₂ problem, *Annu. Rev. Mar. Sci.*, *1*, 169–192.

Eyre, B. D., A. J. Andersson, and T. Cyronak (2014), Benthic coral reef calcium carbonate dissolution in an acidifying ocean, *Nat. Clim. Change*, *4*(11), 969–976.

Feely, R. A., R. H. Byrne, J. G. Acker, P. R. Betzer, C.-T. A. Chen, J. F. Gendron, and M. F. Lamb (1988), Winter-summer variations of calcite and aragonite saturation in the northeast Pacific, *Mar. Chem.*, *25*(3), 227–241.

Feely, R. A., C. L. Sabine, K. Lee, W. Berelson, J. Kleypas, V. J. Fabry, and F. J. Millero (2004), Impact of anthropogenic CO₂ on the CaCO₃ system in the Oceans, *Science*, *305*(5682), 362–366.

Feely, R. A., C. L. Sabine, J. M. Hernandez-Ayon, D. Ianson, and B. Hales (2008), Evidence for upwelling of corrosive "acidified" water onto the continental shelf, *Science*, *320*(5882), 1490–1492.

Feely, R. A., S. R. Alin, J. Newton, C. L. Sabine, M. Warner, A. Devol, C. Krembs, and C. Maloy (2010), The combined effects of ocean acidification, mixing, and respiration on pH and carbonate saturation in an urbanized estuary, *Estuarine Coastal Shelf Sci.*, *88*(4), 442–449.

Fennel, K. (2010), The role of continental shelves in nitrogen and carbon cycling: Northwestern North Atlantic case study, *Ocean Sci.*, *6*(2), 539–548.

Friis, K., A. Kortzinger, and D. W. R. Wallace (2003), The salinity normalization of marine inorganic carbon chemistry data, *Geophys. Res. Lett.*, *30*(2), 1085, doi:10.1029/2002GL015898.

Gledhill, D. K., et al. (2015), Ocean and coastal acidification off New England and Nova Scotia, *Oceanography*, *28*(2), 182–197.

Goldman, J. C., and P. G. Brewer (1980), Effect of nitrogen-source and growth-rate on phytoplankton-mediated changes in alkalinity, *Limnol. Oceanogr.*, *25*(2), 352–357.

Hales, B., W. J. Cai, B. Mitchell, C. Sabine, and O. Schofield (2008), *North American Continental Margins: A synthesis and planning workshop. Report of the North American Continental Margins Working Group for the U.S. Carbon Cycle Scientific Group and Interagency Working Group*, pp. 3–13, U.S. Carbon Cycles Science Program, Washington, D. C.

Hayashi, K. (2014), *Biogeochmical Particle Flux, Resuspension and Deposition in the Western Gulf of Maine*, 85 pp., Univ. of Mass. Dartmouth, New Bedford.

Hsiao, S. C. T. (1939), The reproduction of Limacina retroversa (Flem.), *Biol. Bull.*, *76*, 280–303.

Hunt, B. P. V., E. A. Pakhomov, G. W. Hosie, V. Siegel, P. Ward, and K. Bernard (2008), Pteropods in Southern Ocean ecosystems, *Prog. Oceanogr.*, *78*(3), 193–221.

Hunt, C. W., J. E. Salisbury, D. Vandemark, and W. McGillis (2011), Contrasting carbon dioxide inputs and exchange in three adjacent New England estuaries, *Estuaries Coasts*, *34*(1), 68–77.

Jiang, M. S., M. Zhou, S. P. Libby, and D. M. Anderson (2011), Dynamics of a mesoscale eddy off Cape Ann, Massachusetts in May 2005, *Deep Sea Res., Part I*, *58*(11), 1130–1146.

Karnovsky, N. J., K. A. Hobson, S. Iverson, and G. L. Hunt (2008), Seasonal changes in diets of seabirds in the North Water Polynya: A multiple-indicator approach, *Mar. Ecol. Prog. Ser.*, *357*(291), 99.

Keigwin, L. D., and C. H. Pilskaln (2015), Sediment flux and recent paleoclimate in Jordan Basin, Gulf of Maine, *Cont. Shelf Res.*, *96*, 45–55.

Lalli, C. M., and R. W. Gilmer (1989), *Pelagic Snails: The Biology of Holoplanktonic Gastropod Mollusks*, Stanford Univ. Press, Stanford, Calif.

Lischka, S., and U. Riebesell (2012), Synergistic effects of ocean acidification and warming on overwintering pteropods in the Arctic, *Global Change Biol.*, *18*(12), 3517–3528.

McGillicuddy, D. J., M. L. Brosnahan, D. A. Couture, R. He, B. A. Keafer, J. P. Manning, J. L. Martin, C. H. Pilskaln, D. W. Townsend, and D. M. Anderson (2014), A red tide of Alexandrium fundyense in the Gulf of Maine, *Deep Sea Res., Part II*, *103*, 174–184.

McLaughlin, K., et al. (2015), Core principles of the California Current Acidification network linking chemistry, physics, and ecological effects, *Oceanography*, *28*(2), 160–169.

Mehrbach, C. (1973), Measurement of the apparent dissociation constants of carbonic acid in seawater at atmospheric pressure, *Limnol. Oceanogr.*, *18*(6), 897–907.

Millero, F. J. (2007), The marine inorganic carbon cycle, *Chem. Rev.*, *107*(2), 308–341.

Morse, J. W., R. S. Arvidson, and A. Luttge (2007), Calcium carbonate formation and dissolution, *Chem. Rev.*, *107*(2), 342–381.

Najjar, R. G., M. Friedrichs, and W.-J. Cai (2012), *Report of the U.S. East Coast Carbon Cycle Synthesis Workshop*, 34 pp., Ocean Carbon and Bio-geochemistry Program and North American Carbon Program, Virginia Institute of Marine Sciences, Gloucester Point, Va.

Orr, J. C., et al. (2005), Anthropogenic ocean acidification over the twenty-first century and its impact on calcifying organisms, *Nature*, *437*(7059), 681–686.

Pettigrew, N. R., J. H. Churchill, C. D. Janzen, L. J. Mangum, R. P. Signell, A. C. Thomas, D. W. Townsend, J. P. Wallinga, and H. J. Xue (2005), The kinematic and hydrographic structure of the Gulf of Maine Coastal Current, *Deep Sea Res., Part II*, *52*(19-21), 2369–2391.

Pierrot, D., E. Lewis, and D. Wallace (2006), MS Excel program developed for CO2 system calculations, *ORNL/CDIAC-105a*, Carbon Dioxide Inf. Anal. Cent., Oak Ridge Natl. Lab., U.S. Dep. of Energy, Oak Ridge, Tenn.

Pilskaln, C. H., K. Hayashi, B. A. Keafer, D. M. Anderson, and D. J. McGillicuddy (2014a), Benthic nepheloid layers in the Gulf of Maine and Alexandrium cyst inventories, *Deep Sea Res., Part II*, *103*, 55–65.

Pilskaln, C. H., D. M. Anderson, D. J. McGillicuddy, B. A. Keafer, K. Hayashi, and K. Norton (2014b), Spatial and temporal variability of Alexan-drium cyst fluxes in the Gulf of Maine: Relationship to seasonal particle export and resuspension, *Deep Sea Res., Part II*, *103*, 40–54.

Redfield, A. C. (1939), The history of a population of Limacina ret- roversa during its drift across the Gulf of Maine, *Biol. Bull.*, *76*, 26–47.

Riebesell, U., V. J. Fabry, L. Hansson, and J.-P. Gattuso (Eds.) (2010), *Guide to Best Practices for Ocean Acidification Research and Data Report-ing*, 260 pp., Publ. Off. of the Eur. Union, Luxembourg.

Salisbury, J., M. Green, C. Hunt, and J. Campbell (2008a), Coastal acidification by rivers: A threat to shellfish?, *Eos Trans. AGU*, *89*(50), 513–520.

Salisbury, J., D. Vandemark, C. Hunt, J. Campbell, B. Jonsson, A. Mahadevan, W. McGillis, and H. J. Xue (2009), Episodic riverine influence on surface DIC in the coastal Gulf of Maine, *Estuarine Coastal Shelf Sci.*, *82*(1), 108–118.

Salisbury, J. E., D. Vandemark, C. W. Hunt, J. W. Campbell, W. R. McGillis, and W. H. McDowell (2008b), Seasonal observations of surface waters in two Gulf of Maine estuary-plume systems: Relationships between watershed attributes, optical measurements and surface pCO₂, *Estuarine Coastal Shelf Sci.*, *77*(2), 245–252.

Signorini, S. R., A. Mannino, R. G. Najjar, M. A. M. Friedrichs, W. J. Cai, J. Salisbury, Z. A. Wang, H. Thomas, and E. Shadwick (2013), Surface ocean pCO(2) seasonality and sea-air CO2 flux estimates for the North American east coast, *J. Geophys. Res. Oceans*, *118*, 5439–5460, doi:10.1002/jgrc.20369.

Sutton, A. J., et al. (2016), Using present-day observations to detect when anthropogenic change forces surface ocean carbonate chemistry outside pre-industrial bounds, *Biogeosci. Discuss.*, *2016*, 1–30.

Thabet, A. A., A. E. Maas, G. L. Lawson, and A. M. Tarrant (2015), Life cycle and early development of the thecosomatous pteropod *Limacina retroversa* in the Gulf of Maine, including the effect of elevated CO₂ levels, *Mar. Biol.*, *162*(11), 2235–2249.

Thomas, A. C., D. W. Townsend, and R. Weatherbee (2003), Satellite-measured phytoplankton variability in the Gulf of Maine, *Cont. Shelf Res.*, *23*(10), 971–989.

Townsend, D. W., N. D. Rebuck, M. A. Thomas, L. Karp-Boss, and R. M. Gettings (2010), A changing nutrient regime in the Gulf of Maine, *Cont. Shelf Res.*, *30*(7), 820–832.

Townsend, D. W., D. J. McGillicuddy, M. A. Thomas, and N. D. Rebuck (2014), Nutrients and water masses in the Gulf of Maine-Georges Bank region: Variability and importance to blooms of the toxic dinoflagellate Alexandrium fundyense, *Deep Sea Res., Part II*, *103*, 238–263.

Townsend, D. W., N. R. Pettigrew, M. A. Thomas, M. G. Neary, D. J. McGillicuddy, and J. O'Donnell (2015), Water masses and nutrient sources to the Gulf of Maine, *J. Mar. Res.*, *73*(3-4), 93–122.

Turley, C., M. Eby, A. J. Ridgwell, D. N. Schmidt, H. S. Findlay, C. Brownlee, U. Riebesell, V. J. Fabry, R. A. Feely, and J. P. Gattuso (2010), The societal challenge of ocean acidification, *Mar. Pollut. Bull.*, *60*(6), 787–792.

Vandemark, D., J. E. Salisbury, C. W. Hunt, S. M. Shellito, J. D. Irish, W. R. McGillis, C. L. Sabine, and S. M. Maenner (2011), Temporal and spa-tial dynamics of CO₂ air-sea flux in the Gulf of Maine, *J. Geophys. Res.*, *116*, C01012, doi:10.1029/2010JC006408.

Waldbusser, G. G., E. L. Brunner, B. A. Haley, B. Hales, C. J. Langdon, and F. G. Prahl (2013), A developmental and energetic basis linking lar-val oyster shell formation to acidification sensitivity, *Geophys. Res. Lett.*, *40*, 2171–2176, *doi*:10.1002/grl.50449.

Waldbusser, G. G., B. Hales, C. J. Langdon, B. A. Haley, P. Schrader, E. L. Brunner, M. W. Gray, C. A. Miller, and I. Gimenez (2015), Saturation-state sensitivity of marine bivalve larvae to ocean acidification, *Nat. Clim. Change*, *5*(3), 273–280.

Wang, Z. A., and W. J. Cai (2004), Carbon dioxide degassing and inorganic carbon export from a marsh-dominated estuary (the Duplin Riv-er): A marsh CO₂ pump, *Limnol. Oceanogr. Methods*, *49*(2), 341–354.

Wang, Z. A., R. Wanninkhof, W. J. Cai, R. H. Byrne, X. P. Hu, T. H. Peng, and W. J. Huang (2013), The marine inorganic carbon system along the Gulf of Mexico and Atlantic coasts of the United States: Insights from a transregional coastal carbon study, *Limnol. Oceanogr. Methods*, *58*(1), 325–342.

Wanninkhof, R., L. Barbero, R. Byrne, W. J. Cai, W. J. Huang, J. Z. Zhang, M. Baringer, and C. Langdon (2015), Ocean acidification along the Gulf Coast and East Coast of the USA, *Cont. Shelf Res.*, *98*, 54–71.

Wiebe, P. H., A. W. Morton, A. M. Bradley, R. H. Backus, J. E. Craddock, V. Barber, T. J. Cowles, and G. R. Flierl (1985), New developments in the Mocness, an apparatus for sampling zooplankton and micronekton, *Mar. Biol.*, *87*(3), 313–323.

Wolf-Gladrow, D. A., R. E. Zeebe, C. Klaas, A. Kortzinger, and A. G. Dickson (2007), Total alkalinity: The explicit conservative expression and its application to biogeochemical processes, *Mar. Chem.*, *106*(1-2), 287–300.